



The effect of nickel on the mechanical behavior of molybdenum P/M steels

B.A. Gething^a, D.F. Heaney^{a,*}, D.A. Koss^{a,b}, T.J. Mueller^a

^a *The Center for Innovative Sintered Products, 118 Research Building West,
The Pennsylvania State University, University Park, PA 16802, USA*

^b *Department of Materials Science and Engineering, The Pennsylvania State University, University Park, PA, USA*

Received 15 May 2004; received in revised form 23 May 2004

Abstract

This study has examined the effects of nickel alloying additions on the microstructural characteristics and mechanical properties of Fe–xNi–0.85Mo–0.4C-base steels that were powder processed using double-press double-sinter processing to maximize density. The steels were examined in the as-processed condition as well as in a quench-and-temper heat treated condition. Tensile behavior indicates that while nickel content (at levels of 2, 4, and 6%) increased tensile strength in the as-sintered condition, it did not significantly affect tensile strength in the quenched and tempered condition. In both conditions increasing Ni content decreased elongation to fracture. The 4% Ni steel, which tended to have the smallest maximum pore size, also exhibited the greatest fatigue strength.

© 2004 Published by Elsevier B.V.

Keywords: Molybdenum/nickel steels; Pressed and sintered steels; High strength; Double-press double-sintered steels; Tensile strength; Fatigue strength

1. Introduction

For a powder metallurgy (P/M) component to be considered for high performance applications, porosity must be reduced to a minimum; i.e. density must be maximized. Many methods to reduce porosity have been explored, such as the hypopulsor technique [1], warm compaction [2], and high temperature sintering [3]. One of the more common methods to reduce porosity is known as “double-press double-sintering” (DPDS), which decreases bulk porosity of conventional ferrous-based components from approximately 10% after the conventional single-press single-sinter (SPSS) to 5% porosity after DPDS [4,5].

Another method to improve the mechanical properties of P/M materials is through the use of alloy additions. These additions can be pre-alloyed with the iron prior to powder production or added as an elemental powder addition to the base iron powder. For example, a “workhorse” series of alloys for

moderate- to high-stress P/M applications are the P/M grades 4200, 4400 and 4600 series steels, which rely on nickel, carbon, and molybdenum additions. In most cases, the nickel and the carbon are added as elemental powder additions, whereas the molybdenum is pre-alloyed with the base iron powder. Due to the industrial importance of these PM steels, many studies have addressed aspects of their processing and behavior [2–13]. However, each study has used a slightly different alloy or processing method, and comparisons as well as standardized properties are difficult to ascertain. For example, while it is known that strength increases with an increase in nickel content [14], limited elongation data exists. Engstrom and Allroth reported that elongation moderately increases with nickel content, but at nickel contents greater than 6%, which are of lesser interest today [15]. Similarly, Morioka [7,8] examined fatigue strength for 2 and 4% nickel alloys, but each of these alloys had different molybdenum contents and the 4% nickel alloy also contained copper additions. No study has determined tensile and fatigue behavior as a function of nickel content while maintaining constant process and alloy parameters.

* Corresponding author. Tel.: +1 814 865 7346; fax: +1 814 863 8211
E-mail address: dfh100@psu.edu (D.F. Heaney).

58 The objective of this work is to examine the effect of nickel
59 additions on the tensile and fatigue behavior of molybdenum
60 P/M steels. High density processing was applied through
61 DPDS to reduce the effects of porosity, thereby increasing
62 performance and making the effects of the alloy additions
63 more prominent. This study examines the influences of the
64 nickel additions on porosity, microstructure, hardness, tensile
65 strength, and elongation to fracture in both the as-sintered
66 condition and a quenched-and-tempered heat-treated condi-
67 tion; fatigue strength at 10^6 cycles was also determined for
68 the “heat-treated” condition.

69 2. Experimental procedure

70 Samples were fabricated from water-atomized alloy pow-
71 der and elemental additions of nickel and carbon. If nickel
72 and carbon are pre-alloyed with the base iron material, the
73 compressibility is reduced resulting in lower overall density,
74 while the molybdenum has little effect on the compressibility
75 of the base iron powder. The base iron powder was Atomet
76 4401, supplied by Quebec Metal Powders Limited. Atomet
77 4401 is water-atomized, pre-alloyed iron powder consisting
78 of 0.8% Mo and 0.16% Mn on a weight basis. The iron pow-
79 der had a rounded but irregular shape with a mean powder
80 particle size of 37 μm . The elemental nickel powder, No-
81 vamet Type 123, had a mean particle size of 8 μm and was
82 spherical and sponge-like in appearance.

83 Carbon from Asbury Graphite Mills Inc., (PM 5) was
84 added in the form of graphite. The initial admixed carbon
85 amount was 0.46 wt.% which resulted in a nominal post-
86 sintered composition of 0.40%. This reduction of 0.06% dur-
87 ing sintering is believed to result from the carbon reduction
88 of the oxide layer on the Atomet 4401 powder, and thus, the
89 carbon content identified for the alloys in this study refers
90 to post-sintered carbon content. Typically, prior studies often
91 do not differentiate from pre- and post-sintered carbon con-
92 tent. It will be assumed that a pre-sintered carbon content of
93 0.5% in prior studies is comparable to the post-sintered 0.4%
94 carbon content in the present study, as some decarburization
95 during the sintering process is likely.

96 A lubricant, Acrawax “C,” in the amount of 0.5 wt.% was
97 also added to the alloy mixtures. A total of 100 g was mixed
98 for each alloy in a Glen Mills Inc., turbula mixer for 30 min,
99 with the rotation speed set at 50 rpm.

100 Two different geometries of samples for mechanical
101 testing were used for the study. Standard P/M dog-bone
102 tensile bars were powder processed to the MPIF Stan-
103 dard 10 geometry, with a thickness of approximately
104 0.65 cm. After sintering, the section for quenched and
105 tempered specimens was reduced by machining to ap-
106 proximately half the original width. This modification in-
107 creased the stress in the gage section to ensure frac-
108 ture in the gauge section and to eliminate grip slip-
109 page, which was a problem in the unmodified samples.
110 Four-point-bend fatigue bars were fabricated to the MPIF

Standard 40 geometry, with a thickness of approximately 111
0.45 cm. 112

113 All samples were initially pressed at 550 MPa and subse-
114 quently pre-sintered in an Inconel Lindberg retort furnace by
115 being heated to 450 °C at 5 °C/min and held for 180 min for
116 lubricant burnout, then being heated to 750 °C at 10 °C/min
117 and held for 30 min in flowing 10% hydrogen/90% nitrogen
118 atmosphere to pre-sinter and anneal the samples, and then fur-
119 nace cooled at a rate of approximately 15 °C/min. All samples
120 were then pressed a second time at 825 MPa. A resizing die
121 was used for the second pressing of the tensile specimens. The
122 opening of the die was larger than the initial die by 0.127 mm
123 in all directions, allowing for easier part entry to the die.
124 The walls were tapered by the 0.127 mm over a distance of
125 1.27 cm so that the inside of the die was the same size as the
126 initial die. Before the samples were pressed a second time,
127 they were lightly sprayed with zinc stearate to reduce friction
128 effects. High temperature sintering was performed in a CM
129 333 pusher furnace at a temperature of 1288 °C and a time of
130 60 min. A sintering atmosphere of 50% H₂ and 50% N₂ was
131 used. Specimens were air cooled in the furnace cooling zone
132 at an undetermined cooling rate.

133 After the double-press double-sinter processing, half of
134 the samples from the study were heat treated by austenitizing
135 at 870 °C (1600 F) at a 0.7% C potential in an endothermic at-
136 mosphere for 60 min and then quenched in oil. These samples
137 were subsequently tempered for 60 min at 390 °C in an N₂
138 atmosphere. This temperature represents the upper range of
139 temperatures used to temper high-strength powder-processed
140 steels [3–12,16] in order to ensure that the specimens regained
141 the maximum amount of tensile ductility.

142 The Archimedes technique was used to measure the den-
143 sity of all samples, while the percent porosity was measured
144 using an AccuPyc 1330 pycnometer. Using this technique,
145 samples were compacted and pre-sintered, then crushed into
146 small fragments. These fragments were then measured for
147 density using the pycnometer; this density was utilized as the
148 theoretical density. Comparing this value to the Archimedes
149 values yielded the percent porosity.

150 Hardness measurements were taken using an LR-Series
151 Rockwell-Type hardness indenter. Both Rockwell “B” and
152 “C” scale measurements were taken. Microhardness of indi-
153 vidual steel phases was measured using a Leco M-400H-0
154 testing apparatus using a Vickers diamond indenter. The ten-
155 sile strengths were measured using an Instron 4100 tensile
156 tester, at a strain rate of 10^{-2} s.

157 Fatigue strength at 10^6 cycles was measured using the
158 four-point-bend test fixture described above [17]. The fixture
159 was equipped with pins that allow for two directions of ar-
160 ticulation to minimize stress concentrations during testing.
161 Fatigue testing was performed using a MTS 1036 Materials
162 Testing machine under load control with a stress ratio (*R*)
163 of 0.1. All samples were tested at a frequency of 30 Hz at
164 ambient conditions. All specimens were surface conditioned
165 to remove sharpness and imperfections along edges, mini-
166 mizing stress risers that might cause inconsistent mechanical

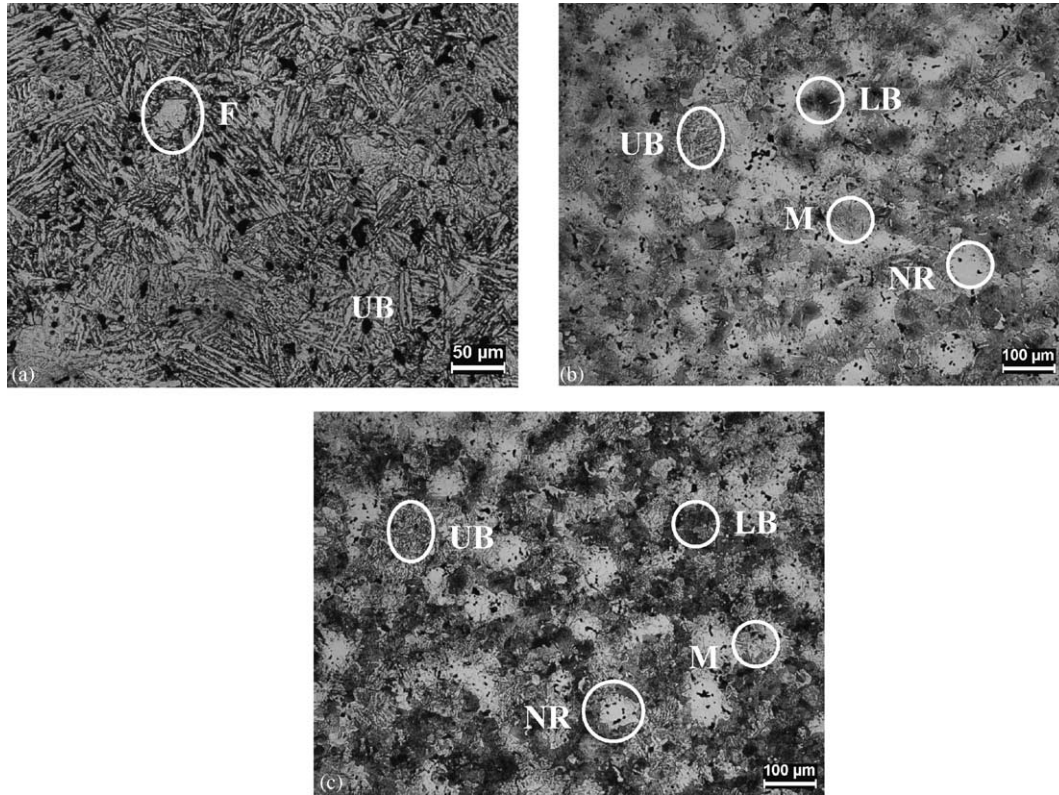


Fig. 1. Optical micrographs of as-sintered Fe-xNi-0.85Mo-0.4C steel containing (a) 2% Ni, (b) 4% Ni, and (c) 6% Ni. The microstructure designations are as follows: UB—upper bainite, F—pro-eutectoid ferrite, M—martensite, LB—lower bainite, and NR—Ni-rich retained austenite.

167 performance. Samples were placed in a vibratory polisher for
 168 10 h. The polisher operates by vibrating samples and milling
 169 media together in a bell-shaped bowl. As these objects vi-
 170 brate, they tumble onto one another, smoothing the surface
 171 and edges.

172 In order to determine the fatigue strength of materials at
 173 10^6 cycles, a staircase method was employed [18]. For this
 174 procedure, the fatigue strength was first estimated based on
 175 prior results by Morioka [8], and the first test was run at this
 176 stress amplitude. If the specimen did not fail at this stress
 177 level, the next test was run at a higher level, and the converse
 178 was performed if the specimen failed. The test procedure con-
 179 tinued in this fashion with stress levels being raised and low-
 180 ered for sequential test specimens. Increments of 20 MPa, ap-
 181 proximately 5% of the estimated fatigue strength, were used
 182 for all staircase tests, and approximately 15 specimens were
 183 tested for each condition to determine the average fatigue
 184 strength at 10^6 cycles in a statistically reliable manner. The
 185 average fatigue strength (S) was determined by using only
 186 the failure or survival specimens, depending on which had
 187 the smaller total. The mean fatigue strength and standard de-
 188 viation (s) were calculated by using the following equations
 189 from Lipson and Sheth [18].

$$190 \bar{S} = S_0 + \left[\frac{A}{\sum n_i} \pm \frac{1}{2} \right] \quad (1)$$

$$s = 1.62d \left[\frac{B \sum n_i - A^2}{\sum (n_i)^2} + 0.029 \right] \quad (2) \quad 191$$

192 In the above equations, S_0 is the lowest stress level during a
 193 particular staircase test, and d the interval spacing or differ-
 194 ence of stress between two steps of the staircase. According
 195 to Lipson and Sheth, the value for d should not exceed 10%
 196 of S_0 . A and B are parameters based on specimen responses.
 197 The stress levels are given coded scores i , where $i = 0$
 198 for the lowest stress level, and n_i is the number of failures (or
 199 survivals) for a given staircase test. In Eq. (1) “+1/2” is used
 200 if survivals are less frequent and “-1/2” if survivals are more
 201 frequent.

202 3. Results and discussion

203 3.1. Microstructural characteristics

204 The microstructures of several alloys were examined to
 205 determine the phases present in both the as-sintered and
 206 heat-treated conditions. In the as-sintered condition shown
 207 in Fig. 1a, the microstructure of the 2% Ni steel is primar-
 208 ily upper bainite (UB) (Vickers hardness value, HVN = 209)
 209 with small, discontinuous regions of randomly dispersed, soft
 210 (HVN = 139) regions believed to be pro-eutectoid ferrite (F).

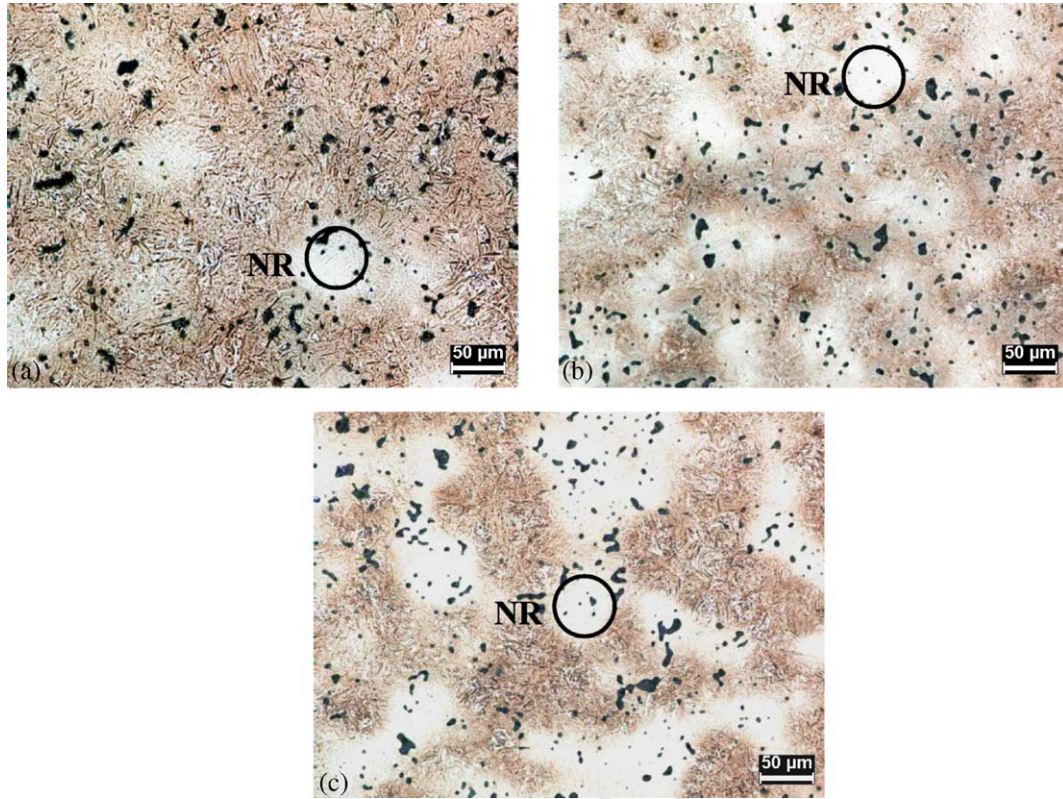


Fig. 2. Optical micrographs of quenched and tempered (a) 2% Ni alloy, (b) 4% Ni alloy, and (c) 6% Ni alloy. NR denotes regions that are primarily Ni-rich retained austenite.

211 The upper bainite regions are comparatively soft when compared to previous results [19]; this softening could be a result of tempering of the upper bainite region during the slow cooling process after sintering.

215 The microstructures of the 4% Ni and 6% Ni alloys in the as-sintered conditions, Fig. 1b and c, are similar to those observed by Kosko in a PM steel with similar composition [5], although no lamellar pearlite regions were observed in the present case. The microstructure also includes regions of upper bainite (UB) (HVN = 248) as well as lower bainite (LB) (HVN = 370) and areas of a needle-like, very hard (HVN = 575) martensite (M) phase. All three of these constituents appear to form in random locations. In addition, a soft (HVN = 180), nickel-rich austenite (NR) is also present; it contains many secondary pores that were formed when the nickel particles dissolved in the iron matrix. The regions of

227 hard martensite and bainite are more prevalent in the 6% Ni alloy. 228

229 After the quench-and-temper heat treatment, the microstructures of all three steels consist primarily of tempered martensite with minor levels of Ni-rich retained austenite; see Fig. 2. The amount of retained austenite phase increases with increasing Ni content, as expected. 230 231 232 233 234

235 The average porosity values were determined from five replicates of each alloy, and the results are shown in Tables 1 and 2. Both the green and DPDS porosity levels were the highest for the 6% Ni alloy, lowest for the 4% Ni, and intermediate for the 2% Ni alloy. One would expect a decrease in porosity of the alloy as the nickel content is increased since the nickel powder is finer and would be more prone to sinter densification. On the other hand, densification 236 237 238 239 240 241

Table 1

Green and sintered densities of (Fe–xNi) alloys investigated in this study (error is standard deviation)

Alloy	Green porosity (%)	DPDS porosity (%)	Densification
(Fe–2Ni)–0.85Mo–0.4C	10.62 ± 0.05	3.57 ± 0.01	7.05 ± 0.06
(Fe–4Ni)–0.85Mo–0.4C	10.93 ± 0.06	3.24 ± 0.02	7.69 ± 0.08
(Fe–6Ni)–0.85Mo–0.4C	11.62 ± 0.05	3.79 ± 0.02	7.83 ± 0.07

Table 2
Mechanical properties of Fe–xNi steels investigated in this study (error is standard deviation)

Alloy	Hardness	Tensile strength (MPa)	Elongation (%)	Fatigue strength at 10 ⁶ cycles
As-sintered properties				
(Fe–2Ni)–0.85Mo–0.4C	81±2 (HRB)	642 ± 8	8.7 ± 0.5	
(Fe–4Ni)–0.85Mo–0.4C	99±3 (HRB)	760 ± 24	6.2 ± 0.7	
(Fe–6Ni)–0.85Mo–0.4C	108±3 (HRB)	943 ± 21	5.0 ± 0.9	
Quenched-and-tempered properties				
(Fe–2Ni)–0.85Mo–0.4C	48 ± 1 (HRC)	1530 ± 14	1.9 ± 0.1	373 ± 6
(Fe–4Ni)–0.85Mo–0.4C	48 ± 1 (HRC)	1551 ± 27	0.9 ± 0.2	396 ± 26
(Fe–4Ni)–0.85Mo–0.4C	49 ± 1 (HRC)	1579 ± 25	0.8 ± 0.2	361 ± 19

of the cold-pressed compact during DPDS decreases with increasing amounts of Ni, as also observed elsewhere [20]. Thus, steels with low Ni additions have high compressibility but low densification, and high-Ni-content steels have low compressibility with high densification, as shown in Table 2. The result is the 4% Ni alloy exhibiting the lowest amount of final porosity, possessing both adequate compressibility and densification.

3.2. Mechanical properties: tensile behavior

As indicated in Table 2, increasing Ni content causes an increase in both the hardness and tensile strength in the as-sintered condition. For example, tensile strength increases from 642 to 943 MPa as Ni content increases from 2% to 6%. The increasing strength and hardness of alloys with higher

Ni content results in a subsequent decrease in elongation for these alloys; tensile elongation is highest at 2% Ni (8.7%), and decreases to 5.0% at 6% Ni content.

In contrast to the behavior in the as-sintered condition, Ni content has only a minor effect on the hardness and tensile strength in the quenched and tempered condition with all three alloys having tensile strength of ≈1550 MPa; see Table 2. The 2% Ni alloy exhibits the highest elongation at 1.9%, while the 4 and 6% Ni alloys exhibit elongations of 0.9 and 0.8%, respectively, for the heat-treated condition.

A comparison of these results with those previously observed for similar PM steels in the quenched and tempered condition is shown in Table 3. Prior studies often do not differentiate between pre- and post-sintered carbon content, and it will be assumed that a pre-sintered carbon content of 0.5% in prior studies is comparable to the post-sintered 0.4% carbon

Table 3
A comparison of the present results with those obtained in prior studies

Study (alloy)	Density (g/cm ³)	Tensile strength (MPa)	Elongation (%)	Bending fatigue strength at 10 ⁶ cycles (MPa)	Processing and chemistry comments
Present (Fe–2Ni)–0.85Mo–0.4C	7.50	1530	1.9	373	DPDS
Narasimhan: [2]	7.20	1300	N/A	N/A	Lower density
(Fe–1.8Ni)–0.5Mo–0.5C					
Hanada: [7]	7.47	1711	N/A	N/A	Pre-alloyed powder
(Fe–0.5Ni)–0.5Mo–0.5C					
Hanada: [7]	7.50	1946	N/A	N/A	Diffusion bonded powder
(Fe–2Ni)–1.0Mo–0.5C					
Morioka: [7]	7.48	2000 approximately	N/A	420 approximately 10 ⁶ cycles	Diffusion bonded powder–higher C content
(Fe–2Ni)–1.0Mo–0.6C					
Furukimi: [6]	7.43	1920	N/A	N/A	Diffusion bonded powder–higher C content
(Fe–2Ni)–1.0Mo–0.6C					
Present (Fe–4Ni)–0.85Mo–0.4C	7.54	1551	0.9	395	DPDS
Hanada: [7]	7.50	1203	N/A	N/A	Cu addition
(Fe–4Ni)–1.5Cu–0.5Mo–0.5C					
Morioka: [8]	7.41	1700 approximately	N/A	350 approximately 10 ⁶ cycles	Cu addition–higher C content
(Fe–4Ni)–1.5Cu–0.5Mo–0.6C					
Present (Fe–6Ni)–0.85Mo–0.4C	7.55	1579	0.8	361	DPDS
Narasimhan: [2]	7.42	1345	N/A	N/A	Warm compaction–lower density:
(Fe–6Ni)–0.85Mo–0.5C					
Narasimhan: [2]	7.42	1400	N/A	N/A	Warm compaction–lower density:
(Fe–6Ni)–1.5Mo–0.5C					

All results are in the quench-and-tempered condition, however, temper temperatures may vary. The last column in the table identifies a difference in processing compared to the present study that could significantly affect the results.

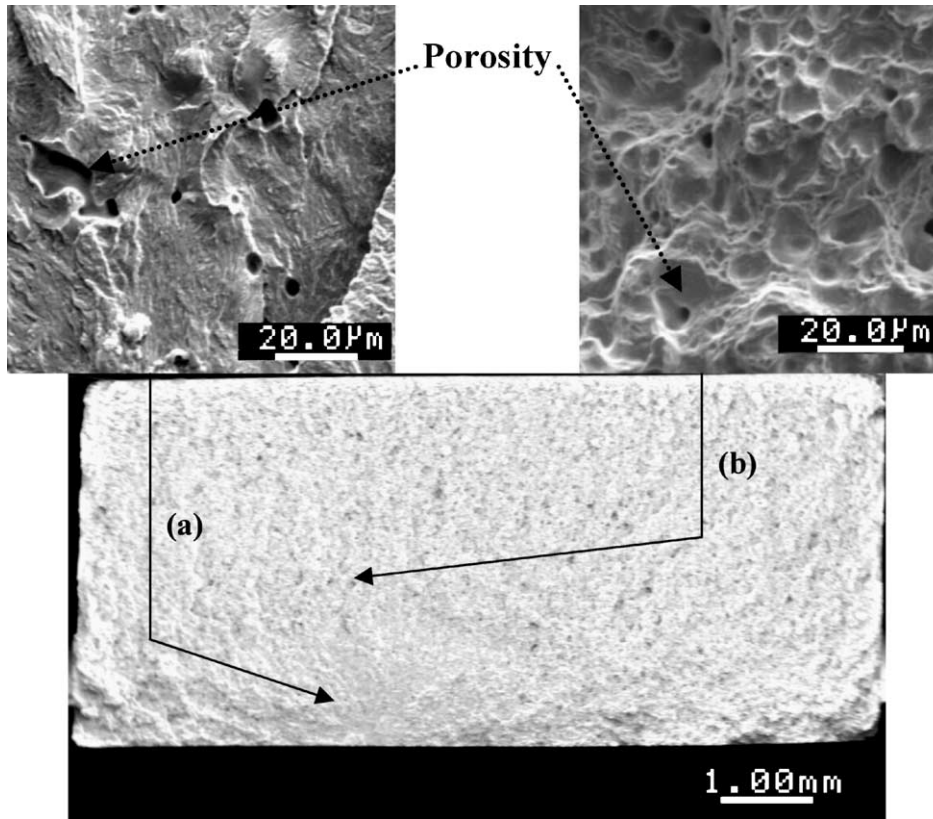


Fig. 3. SEM micrographs of fatigue specimen fracture surface, showing (a) ductile tensile fracture and (b) fatigue fracture regions. Porosity is indicated with dotted arrows.

271 content in the present study, as some decarburization during
 272 the sintering process is likely. Compared to previous studies
 273 at similar density levels [2,8,13], the 2% Ni alloy tested in
 274 this study had a lower strength. The primary reason for the
 275 lower strength was the use of elemental, admixed Ni as ap-
 276 posed to pre-alloyed or diffusion bonded Ni, resulting in soft
 277 (and larger) Ni-rich regions.

278 Another possible reason for the lower strength of this study
 279 is that the temper temperature of this study was 390 °C, which
 280 is the highest accepted tempering temperature for these alloys
 281 and is higher than most of the other studies. The 4% Ni alloy
 282 exhibits a strength that is mid-range in value when compared
 283 to previous studies. For example, the strength results of this
 284 study were higher in comparison to Hanada et al. [7] because
 285 Cu additions tend to decrease the “heat-treated” strength [6].
 286 On the other hand, tensile strengths attained in this study
 287 were lower than those of Furukimi et al. at 2% Ni [6]. Cu
 288 additions were also present in the study of Furukimi and co-
 289 workers, but the carbon content was higher and the temper
 290 temperature was lower, which can result in higher strengths.
 291 For the 6% Ni alloy, no direct comparisons for DPDS are
 292 available, but other high density processing (i.e. warm com-
 293 paction) was performed on 6% nickel steels [2]. The 6% Ni
 294 alloy of this study displayed a higher strength in comparison
 295 to the Narasimhan study [2], mainly due to higher density.
 296 The Narasimhan study offers a direct basis of comparison in

297 terms of alloying, because admixed Ni additions were made
 298 to the alloy, as was the case for the present study. In general,
 299 the results of this study are similar to previous results of simi-
 300 lar studies; therefore, the fatigue data of the following section
 301 should also be representative of this class of P/M steels.

3.3. Mechanical properties: fatigue behavior 302

303 Fatigue tests were performed on the three alloys in the
 304 quenched and tempered conditions, and the results of the
 305 staircase tests appear in Table 2. In all cases, the ratio
 306 of fatigue strength to tensile strength was in the range of
 307 0.23–0.25. The 4% Ni alloy shows the highest average fa-
 308 tigue strength of approximately 395 MPa, while the 2% Ni
 309 alloy exhibits intermediate fatigue strength of approximately
 310 373 MPa. The 6% Ni alloy, which had the highest tensile
 311 strength and porosity level (Table 2), exhibited the lowest fa-
 312 tigue strength of 361 MPa. This behavior is consistent with
 313 other studies that show porosity in P/M alloys decreases fa-
 314 tigue strength significantly [21–23]. It should be noted that,
 315 given the scale of the standard deviations of the fatigue
 316 strengths, the differences between the fatigue strengths of
 317 the alloys are small.

318 The present fatigue results may be compared with those of
 319 Morioka, who examined a 2% Ni alloy with 0.6% C (as op-
 320 posed to 0.4% C here) and processed using diffusion bonded

Table 4

Analysis of the projected pore content on the fracture surface of (Fe–2Ni) P/M steel, where both fatigue and ductile fracture modes were observed

Fracture surface	Approximate crack length (mm)	Porosity on fracture surface (%)	Ratio to bulk porosity
Fatigue crack region	0.5	11.4 ± 1.2	2.4 ± 0.3
Ductile fracture region	3.0	33.7 ± 0.6	7.2 ± 0.2

powders [8], rather than elemental Ni in our case. As shown in Table 3, while the 2% Ni alloy of this study has a lower fatigue strength, it exhibits a slightly higher fatigue strength to tensile strength ratio, 0.24, than that of Morioka who obtained a ratio of 0.21. For the 4% Ni alloy, the fatigue strength was higher than that found by Morioka. As with the 2% Ni alloy, the tensile strength to fatigue strength ratio was also higher, 0.25 compared to 0.21, respectively.

3.4. On the effects of porosity on tensile and fatigue properties

In this study, porosity has shown to decrease both tensile and fatigue strengths of the heat-treated P/M steels, as expected. To explore the influence of porosity on these different modes of fracture, the fracture surfaces were examined to determine the relative levels of porosity on the fatigue and tensile fracture surfaces. As shown in Fig. 3, the fracture surfaces of the quenched and tempered fatigue specimens were analyzed for projected area fraction of porosity, and the results are shown in Table 4.

Quantification of porosity was performed via image analysis by means similar to Danninger et al. [24], although fracture was not performed at low temperatures which would have prevented ductile deformation. Despite this fact, the sintered compacts showed little ductility and any miscalculation due to deformation can be reflected in the error reported with each value. The Danninger study focused on the effective load bearing cross-section (A_c) of the fracture surface, which is a parameter used to predict tensile and fatigue strength of sintered compacts. The present study focuses on the pore content of the fracture surface and how it changes with crack growth phenomena. Surface porosity and A_c are direct opposites of each other.

The amount of porosity on the ductile tensile fracture surface is ≈ 7.2 times that of the bulk porosity or roughly one-third of the fracture surface as viewed in Fig. 3. In contrast, the area fraction of porosity on the fatigue fracture surface was much lower at ≈ 2.4 times the bulk porosity. The implication is that crack growth associated with tensile fracture follows a rough, irregular plane of high pore content. In contrast, fatigue crack growth is much less dependent on porosity, which is consistent with earlier observations that porosity has only a small effect on fatigue crack propagation rates [25]. Thus, the fracture surface of the fatigue crack region is less dependent on porosity and contains a smaller number of pores.

The higher degree of pore participation in tensile crack growth can be understood in terms of the relative scales of the crack-tip plastic zones when compared to the scale of the

pore microstructure. In a tensile test, plasticity within the entire specimen gauge volume is the driving force; the eventual fracture path is one of high pore content and is tortuous and zigzagged in nature [26]. For crack growth processes, plasticity and damage is confined to the crack-tip plastic zone. For crack lengths in Table 4 and correcting for the differences between cyclic and monotonic plastic zone sizes, the plastic zone, r_p , will be approximately 24 times larger for the tensile fracture stage of crack growth than for the fatigue fracture portion [27]. Since damage is confined to a plane $\pm r_p$ of the main crack, only a comparatively small number of pores can participate in the fatigue crack growth process. In contrast, the tensile overload region, r_p , is large and pore participation in the tensile crack growth process is about 3 times greater (Table 4). As a result, the fatigue fracture surface is comparatively flat, as fewer pores cause crack deviation, and it also contains a lower fraction of porosity.

The effect of pore size on the fatigue strength was also investigated in this study. An analysis of the distribution of pore sizes shows that the 4% Ni steel, which had the highest fatigue strength (Table 2), also had the smallest percentage of pores larger than either 10 μm or 20 μm . Thus, as has been observed in the influence of porosity on fatigue of castings, large pores can significantly reduce high cycle fatigue strength [28]. With the smallest fraction of large pores, the 4% Ni alloy will have the smallest likelihood to initiate a long fatigue crack, consistent with its highest fatigue strength.

4. Conclusions

The influence of Ni content (2, 4, and 6 wt.% levels) on the microstructure and mechanical properties has been examined in a series of Fe–xNi–0.85Mo–0.4C steels fabricated by powder metallurgy using elemental Ni additions, relying on a double-press double-sinter processing route to increase density. The results indicate that in the *as-sintered condition* increasing nickel content increases tensile strength and decreases elongation to fracture as a result of increased levels of hard constituents (martensite and lower bainite) within the microstructure. In contrast, after the quench-and-temper heat treatment, Ni additions have no significant effect on tensile strength but decrease elongation slightly for the tempered martensitic structures. Fatigue results for quenched and tempered conditions indicate that the 4% Ni steel has the highest fatigue strength at 10^6 cycles, consistent with the lowest level of large ($>20 \mu\text{m}$) pores in this case.

Acknowledgements

The authors wish to thank The Center for Innovative Sintered Products for supporting this effort under BFTDA Grant No. 21-116-0011. Insightful discussions with John Kosko of Keystone Powdered Metal Company, Edmond Ilia of Metal-dyne Sintered Components, and Francois Chagnon of Quebec Metal Powders Limited are also acknowledged.

References

- [1] Y. Bergstrom, L. Troive, Nord. Steel Min. Rev. 3 (1999) 126.
- [2] K. Narassimhan, J. Tengzelius, Adv. Powder Metall. Part Mater. 5 (1992) 153.
- [3] J. Hamill, R. Causton, O. Shuresh, Adv. Powder Metall. Part Mater. 5 (1992) 193.
- [4] F. Gosselin, M. Gangne, Y. Trudel, Adv. Powder Metall. Part Mater. 5 (1992) 127.
- [5] J. Kosko, in: W.B. Eisen, B.L. Ferguson, R.M. German, R. Iacocca, P.W. Lee, D. Madan, K. Moyer, H. Sanderow, Y. Trudel (Eds.), ASM Handbook: Powder Metal Technologies and Applications, vol. 07, Materials Park, OH, 1998. p. 751.
- [6] O. Furukimi, K. Yano, S. Takajo, Adv. Powder Metall. 5 (1991) 59.
- [7] M. Hanada, N. Motooka, T. Honda, Adv. Powder Metall. Part Mater. 5 (1992) 215.
- [8] Y. Morioka, Met. Powder Rep. 45 (1990) 181.
- [9] F. Hanejko, H. Rutz, U. Engstrom, B. Johansson, Adv. Powder Metall. Part Mater. 10 (1995) 77.
- [10] H. Khorsand, H. Yoozhashizade, S.M. Habibi, K. Janghorban, A. Nangir, S. Reihani, Met. Powder Rep. 57 (2002) 32.
- [11] J.J. Horn, R.I. Stephens, T. Prucher, Powder Metall. 41 (1998) 205.
- [12] W.B. James, M.C. Baran, F.J. Semel, R.J. Causton, K.S. Narasimhan, Proceedings from Euro2000, Budapest, Hungary, July, 2000.
- [13] A. Graham, T. Cimino, A. Rawlings, H. Rutz, Adv. Powder Metall. Part Mater. 13 (1997) 75.
- [14] L. Pease, Int. J. Powder Metall. 37 (2001) 28.
- [15] U. Engstrom, S. Allroth, Proceedings from Powder Metall. World Congress Part II, Dusseldorf, Germany, 1986, p. 1039.
- [16] W. Jamesin, W.B. Eisen, B.L. Ferguson, R.M. German, R. Iacocca, P.W. Lee, D. Madan, K. Moyer, H. Sanderow, Y. Trudel (Eds.), ASM Handbook: Powder Metal Technologies and Applications, vol. 07, Materials Park, OH, 1998. p. 947.
- [17] B. Gething, M.S. Thesis, Pennsylvania State University, University Park, PA, 2003.
- [18] C. Lipson, N. Sheth, Statistical Design and Analysis of Engineering Experiments, McGraw-Hill, New York, 1973.
- [19] L. Samuels, Optical Microscopy of Carbon Steels, ASM International, Metals Park, OH, 1980.
- [20] F. Chagnon, Y. Trudel, Adv. Powder Metall. Part Mater. 5 (1995) 3.
- [21] S. Polasik, N. Chawla, Proceedings from the 2002 International Conference on Powder Metallurgy and Particulate Materials, Orlando, FL, June, 2002.
- [22] T. Cimino, A. Graham, T. Murphy, Adv. Powder Metall. Part Mater. 13 (1998) 33.
- [23] T. Cimino, A. Graham, T. Murphy, A. Lawley, Adv. Powder Metall. Part Mater. 7 (1999) 65.
- [24] H. Danninger, U. Sonntag, B. Kuhnert, R. Ratzi, Prakt. Metallogr. 39 (2002) 8.
- [25] R.A. Queeney, P.S. Dasgupta, Int. J. Fatigue 2 (1980) 113.
- [26] H.J. Niu, I.T. Chang, Scr. Metall. 41 (1999) 481.
- [27] S. Suresh, Fatigue of Materials, Cambridge Press, Cambridge, UK, 1991.
- [28] Q.G. Wang, P.N. Crepeau, D. Gloria, S. Valtierra, Adv. Aluminum Cast. Tech. II (2002) 209.